Kinetic Monte Carlo Study on Carbon Trapping Effect with Pre-amorphized Silicon

Soon-Yeol Park, Young-Kyu Kim, and Taeyoung Won

Department of Electrical Engineering, School of Information Technology Engineering,
Inha University, Incheon, Korea 402-751
twon@hsel.inha.ac.kr

ABSTRACT

We report our kinetic Monte Carlo (kMC) study of the impact of carbon co-implant on the pre-amorphization implant (PAI) process. We employed both BCA (Binary Collision Approximation) approach for the acquisition of the initial *as-implant* dopant profile and kMC method for the simulation of diffusion process during the annealing process. Our simulation study revealed that carbon co-implant process efficiently suppresses the boron diffusion due to the annihilation of interstitials. In addition, we looked into the boron diffusion under the influence of carbon through calculating the carbon reaction with interstitials. Our kMC study implied that the energy of the carbon co-implant influences the boron diffusion due to the enhancement of trapping occurrences of interstitials with boron.

Keywords: carbon co-implant, pre-amorphization, binary collision approximation, kinetic monte carlo

1 INTRODUCTION

As the MOSFET (Metal Oxide Semiconductor Field Effect Transistor) scales down to sub-nanometer regime, it becomes more stringent and mandatory to implement an ultra shallow junction in order to mitigate a short channel effect [1-3]. In order to achieve an ultra shallow junction, we have to take measures both in the ion implantation process and in the subsequent annealing process. In the ion implantation process, we have to suppress the channeling phenomena wherein implanted species penetrate deeply into the silicon. It is also well known in the art that dopant diffusion during the subsequent annealing process deepens the junction depth, which is called transient enhanced diffusion (TED) [4].

Several approaches have been employed in an effort to obtain a shallow junction such as a tilted implantation with respect to the crystalline orientation of the substrate and low-energy implantation energy. Recently, pre-amorphization implant (PAI) technique has been extensively investigated for realizing the ultra shallow junction wherein the PAI changes the silicon lattice configuration into an amorphous state and thereby reduces the channeling phenomena of the implanted atoms. Germanium and silicon atoms have been employed for the pre-amorphization implant with relatively higher level energy than the target doping atoms.

More recently, some studies reported that carbon co-implant after PAI process further effectively reduces TED when compared with the traditional PAI-only process. The effectiveness of the carbon co-implant PAI process seems to come from the fact that carbon clusters with interstitial are formed which suppresses the boron diffusion. Consequently, we have undertaken the numerical study in order to precisely understand the behind physics of the carbon co-implant in PAI process.

2 COMPUTATIONAL DETAILS

Firstly, we need *as-implant* boron profiles for the SI PAI case and the carbon co-implant case in order to investigate the diffusion phenomena of boron for both cases. In this work, we employed the BCA (Binary Collision Approximation) code for the initial *as-implant* dopant profile, which is based on the Kinchin-Pease model, a computationally efficient damage model based on the modified Kinchin-Pease formula of Norgett *et al.* [5]. This model accounts for the generation and accumulation of damages, defect encounters, and amorphization. The basic assumption of the Kinchin-Pease models is the nuclear energy loss which is turned into point defects and the number of Frenkel pairs which is created proportionally to the nuclear energy loss. The nuclear energy loss is locally deposited and induces local defects.

The subsequent thermally activated events are simulated after ion implantation. Here, we assume that the system behaves as a Poisson process if the event is not affected by the previous history throughout all the times. The detailed simulation procedures for the cluster transitions are well addressed in our previous publication [6]. In addition, we should take into account the carbon-interstitial cluster. The diffusion and trapping mechanism of the carbon with interstitial was assumed to be so-called kick-out mechanism as expressed in the following equation (1). Here, C_s denotes a carbon concentration in substitutional position which is assumed to be immobile. Further, C_i denotes a carbon residing in an interstitial position, which is highly mobile. The kick-out model is a very simple, but very precise model which quite coincidently supports the experimental results of silicon self-diffusion [7] and diffusivity of C_i:

$$C_s + I \leftrightarrow C_i \quad (1)$$

This model, however, has a shortcoming because of the difficulty in explaining the vacancy super-saturation which has been experimentally observed in the high-concentrated carbon regions. Recently, Scholz *et al*. [8] argued that an accurate description of the experimental profiles is possible only if the Frank-Turnbull mechanism is additionally taken into account as the following equation (2):

$$C_s \leftrightarrow C_i + V \quad (2)$$

The forward reaction in the Eq. (2) would easily occur and the diffusion of carbon can be explained by the production of C_i, the mobile carbon, which explains the super-saturation of vacancy. We have to calculate the formation of immobile carbon and self-interstitials. At high temperatures carbon has a thermodynamic driving force that leads to the formation of silicon carbide (SiC). However, since the interface energy of SiC-Si is relatively high for the formation of the cluster, simple agglomeration of carbon can happen as an alternative to SiC formation. Consequently, carbon/self-interstitial (C/I) clusters are formed in addition to the diffusion of carbon wherein the reaction of clusters can be expressed as following equations (3) and (4):

$$C_i + C_s \leftrightarrow C_2I \quad (3)$$

The encounter of C_i with C_s results in the C_2I cluster in the forward reaction, which can be broken up to C_i in the reverse reaction. Alternatively, C_2I can be broken to leave an immobile C_2 cluster with interstitial, I, as shown in equation (4):

$$C_2I \leftrightarrow C_2 + I \quad (4)$$

These small clusters can grow rapidly by trapping either I or C_i. The governing reaction of the growth and dissolution of these clusters can be written as the following equations (5) and (6):

$$C_nI_m + C_i \leftrightarrow C_{n+1}I_{m+1} \quad (5)$$

$$C_nI_m + I \leftrightarrow C_nI_{m+1} \quad (6)$$

In addition, we should note that C_nI_m clusters can trap a neighboring silicon atom which is placed in the lattice and release a vacancy (V) as the following equation (7):

$$C_nI_m \leftrightarrow C_nI_{m+1} + V \quad (7)$$

The emission of a vacancy from a C_nI_m cluster is the natural reverse reaction of the trapping of a vacancy, which creates a vacancy diffusing away. It can be regarded as the equivalence of the Frank-Turnbull mechanism wherein C/I clusters replaces C_s. Finally, we can calculate the carbon diffusion profile including the kick-out mechanism, Frank-Turnbull mechanism, and C/I cluster formation mechanism, which has been implemented in our kMC code [9]. The total energies of C_nI_m clusters are shown in Fig. 1. Here, we limited the number of carbon and interstitials for the purpose of computational efficiency. Referring to Fig. 1, we can see that C_9I_9 cluster has enough energy to form the cluster.

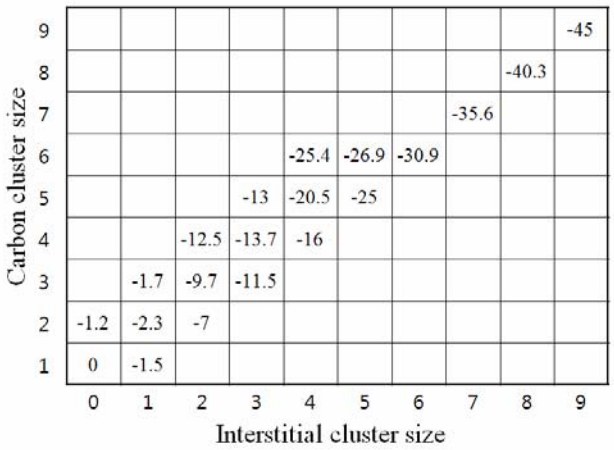

Fig. 1 Total energies of C_nI_m clusters wherein the number of carbon 'n' and interstitial 'm' are limited to 9 for the computational efficiency.

3 RESULTS AND DISCUSSION

As a reference implant profile, boron was implanted with a dosage of 7 x 10^{14} /cm^2 and with energy of 0.5 keV. The Si PAI was simulated with a condition of dosage of 1 x 10^{15} /cm^2 and with energy of 25 keV. Finally, carbon co-implant was performed with a dosage of 1 x 10^{15} /cm^2 and with varying implant energy from 1.5 to 24 keV followed by the Si PAI. We limited the simulation box to 100 nm x 100 nm x 100 nm for most of the cases in order to save the computation time. However, this limitation was released to the case of carbon co-implant to 300 nm x 100 nm x 100 nm because the carbon's projected range exceeds the boundary of 100 nm at high energy implantation. Furthermore, we simulated spike RTA (Rapid Thermal Annealing) at the temperature of 1050˚C for 10 seconds by using kMC code.

Fig. 2 is a schematic diagram which illustrates the *as-implant* profiles and the diffusion profiles for each case in this study. In this figure, empty squares, circles, and triangles denote calculated *as-implant* boron profiles for the case without any PAI, with Si PAI, and with carbon co-implant Si, respectively. We should note that filled squares, circles and triangles correspond to the calculated diffusion profiles after 1050 ˚ C rapid thermal annealing (RTA) for

10 seconds. In the meanwhile, the dotted lines and plain lines denote the experimental SIMS data for the comparison.

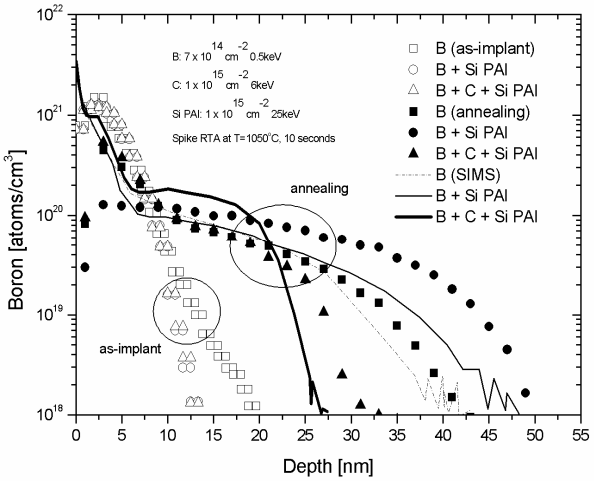

Fig. 2 A schematic diagram which illustrates the *as-implant* profiles and the diffusion profiles for each case in this study.

Referring to the *as-implant* profile in Fig. 2, we can see that both Si PAI (empty circles) and carbon co-implant Si PAI (empty triangles) reduces the channeling of boron when compared with *as-implant* profile without PAI (empty squares), which of course demonstrates the effectiveness of PAI process. If, however, we just look at the *as-implant* profile, we cannot find any vivid evidence of superiority of carbon co-implant Si PAI over the pure Si PAI case. This seems to be due to the negligible difference in the projected range between carbon co-implant Si PAI profile and the Si PAI profile.

In the atomistic modeling of annealing process, interstitial and vacancy profiles are employed for the simulation of dopant diffusion. As is well known, boron tends to diffuse with the assistance of interstitials. Therefore, we investigated the interstitial profile prior to ion implantation and prior to the annealing process. Interestingly, we could find that there exists a difference in the interstitial profile between the carbon co-implant Si PAI case and Si PAI case.

Fig. 3 is a schematic diagram illustrating the interstitial distribution for Si PAI (dotted line) and carbon co-implant Si PAI (solid line). Referring to Fig. 3, we can observe that carbon co-implant Si PAI reduces the amount of interstitials near the surface, which is due to the carbon co-implant wherein the effect of Si PAI is mitigated near the surface when compared with that of Si PAI only sample.

Referring to diffusion profiles (filled circles, squares, and triangles) in Fig. 2, we can see that B profile with Si PAI (filled circles) demonstrates a much deeper penetration depth than that without any co-implant. This seems to be due to excessive interstitials which has been produced from Si PAI. The interstitials then move toward the surface and help the boron diffusion. On the other hand, B + C + Si PAI (filled triangles) show the appreciable suppression of the boron diffusion among these three profiles. Our kMC calculation leads us to come to a conclusion that boron diffusion can be effectively reduced by carbon co-implant Si PAI due to the reduction of interstitials near the surface. Additionally, we confirmed our simulation result by comparing them with SIMS data (experimental). Simulation data seems to be well matched with experimental data.

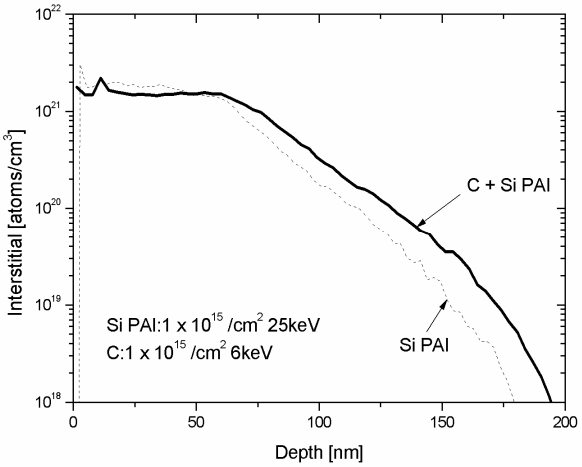

Fig. 3 A schematic diagram illustrating the interstitial distribution for Si PAI (dotted line) and carbon co-implant Si PAI (solid line).

Furthermore, we investigated the carbon profile by kMC during the annealing process in order to figure out what is going on during the boron diffusion process. Fig. 4 is a schematic diagram illustrating the carbon profiles for a variety of implant energy from 1.5 to 24 keV. Referring to Fig. 4, we can see that the carbon penetrates more deeply with implantation energy. Similar to the boron diffusion, carbon also diffuses during the 1050 ˚ C spike RTA regardless of the implantation energies. However, the diffusion tendency of carbon is quite different from the boron as shown in Fig. 4. According to the carbon profile, the peaks of concentration do not change during the annealing process, while the concentration near the surface is reduced a little bit when compared with the boron profile in Fig. 2. We can recognize that carbon diffusion is very limited to the contrary of the boron diffusion. In addition, we can figure out that this phenomenon results from the carbon cluster formation which limits the diffusion of carbon.

Finally, we extracted boron profiles with varying the carbon implantation energies from 1.5 to 24 keV for the purpose of optimizing the carbon co-implant process. Fig. 5 is a schematic diagram illustrating the boron diffusion profiles with carbon co-implant Si PAI with varying carbon implant energies. In this theoretical calculation, we performed Si PAI with dose of 1 x 10^{15} /cm^2 and with energy of 25keV. The carbon co-implant energy ranges from 1.5 to 24 keV with the same dose of 1 x 10^{15} /cm^2. Referring to Fig. 5, we can see that the boron *as-implant* profiles have almost the same distribution for the wide range of carbon implantation energies, which implies that implantation energy of carbon co-implant does not affect the boron implantation channeling in an appreciable manner.

However, we can observe that there exists some kind of optimum point for the diffusion profiles. Referring to Fig. 5, we can see that the diffusion depth is the lowest for 3keV carbon implantation energy. Additionally, our simulation reveals that the boron diffusion is severely widened for 24 keV, which seems to be due to the excessive carbon reaction as an interstitial trap. For 3 keV implantation of carbon, the probability that boron meets interstitial is reduced due to the carbon trapping between boron and interstitial. The difference in the carbon distribution results in the different suppressing effect in the boron diffusion. Our simulation results imply that the effectiveness of carbon co-implant as interstitial trap is maximized at the implantation energy of 3 keV.

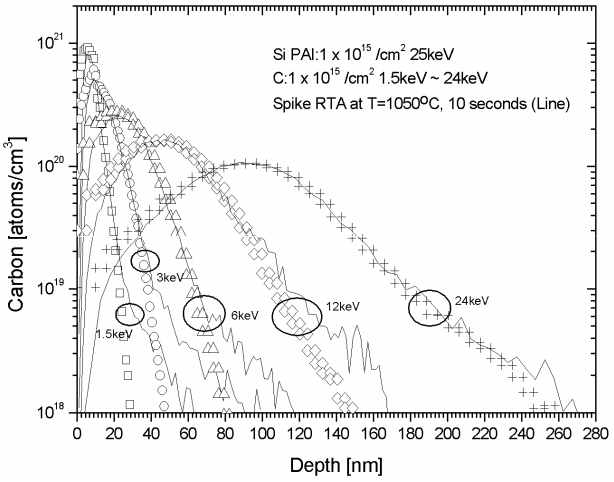

Fig. 4 Carbon *as-implant* and annealing profiles added to Si PAI wherein the empty symbols indicate *as-implant* profile, and the lines indicate annealing profile. Carbon implantation energies are different from 1.5keV to 24keV.

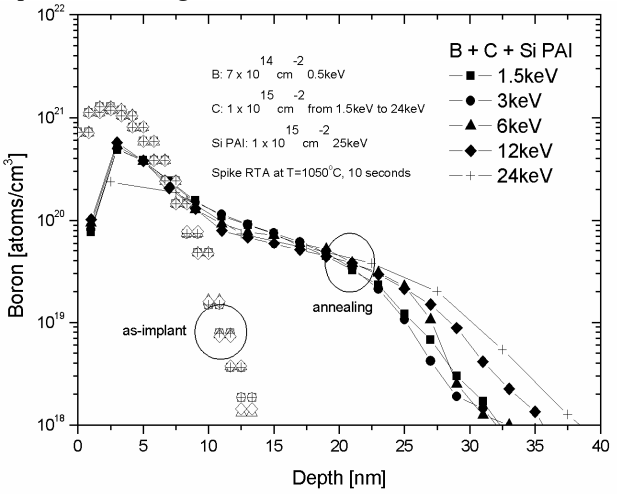

Fig. 5 A schematic diagram illustrating the boron diffusion profiles with carbon co-implant Si PAI with varying carbon implant energies.

4 CONCLUSION

In this work, we investigated the Si PAI process and carbon co-implant Si PAI process in detail by employing BCA (Binary Collision Approximation) and kMC (kinetic Monte Carlo) codes. We calculated damage profiles which are induced by Si PAI and carbon co-implant Si PAI, which are then fed into kMC code for annealing process. The effectiveness of carbon co-implant Si PAI was significantly appreciated by looking into the interstitial distribution as well as the boron diffusion profiles for the different PAI conditions. Finally, the implant energy of carbon was also varied in an effort to optimize the shallow junction profile.

ACKNOWLEDGMENT

This research was supported by the Ministry of Knowledge Economy, Korea, under the ITRC (Information Technology Research Center) support program supervised by the IITA(Institute of Information Technology Advancement) (IITA-2008-C109008010030).

REFERENCES

[1] P. M. Fahey, P. B. Griffin, and J. D. Plummer, Rev Mod. Phys. 61, 289 (1989).
[2] P. A. Stolk, H. Gossmann, D. J. Eanglesham, D. C. Jacobson, C. S. Rafferty, G. H. Gilmer, M. Jaraiz, J. M. Poate, H. S. Luftman, and T. E. Haynes, J. Appl. Phys. 81, 6031 (1977).
[3] A. Agarwal, H. Gossmann, D. J. Eaglesham, S. B. Herner, A. T, Fiory, and T. E. Haynes, J. Appl. Phys. 81, 6031 (1997).
[4] N. E. B. Cowern, G. Mannino, P. A. Stolk, F. Roozeboom, H. G. A. Huizing, J. G. M. van Berkum, F. Cristiano, A. Claverie, and M. Jaraiz, Phys. Rev. Lett. 82, 4460 (1999).
[5] M. J. Norgett. M. T. Robinson, and I. M. Torrens, Nucl. Eng. Des., 33, 50, (1975).
[6] J. Yoo, K. Yoon, J. Kim and T. Won, J. Korean Phys. Soc. 49, pp.1260, (2006).
[7] H. Bracht, E. E. Haller, and R. Clark-Phelps, Phys. Rev. Lett. 81, 393 (1998).
[8] R. F. Scholz, P. Werner, U. Gösele, and T. Y. Tan, Appl. Phys. Lett. 74, 392 (1999).
[9] J. Kim and T. Won, Microelectron. Eng., 84, 1556, (2007).